Parallel and numerical issues of the edge finite element method for 3D controlled-source electromagnetic surveys

Octavio Castillo Reyes, Josep de la Puente, Vladimir Puzyrev, José María Cela
Computer Applications in Science and Engineering (CASE)
Barcelona Supercomputing Center
octavio.castillo@bsc.es

***Abstract*—This paper deals with the most relevant parallel and numerical issues that arise when applying the Edge Element Method in the solution of electromagnetic problems in exploration geophysics. In this sense, in recent years the application of land and marine controlled-source electromagnetic (CSEM) surveys has gained tremendous interest among the offshore exploration community. This method is especially significant in detecting hydrocarbon in shallow/deep waters. On the other hand, in Finite Element Methods for solving electromagnetic field problems, the use of Edge Elements has become very popular. In fact, Edge Elements are often said to be a cure to many difficulties that are encountered (particularly eliminating spurious solutions) and are claimed to yield accurate results. CSEM, linear vectorial edge basis functions and its implementation on unstructured tetrahedral meshes are discussed. The use of it's kind of discretisation enables the representation of complex geological structures and allows local refinement in order to improve the solution's accuracy. A parallel shared memory approach is proposed to meet the high computational cost of EM modeling. Performance results and an convergence study are presented in order to validate our numerical method.**

***Index Terms*—Parallel computing, share memory, exploration geophysics, edge-based finite element.**

I. Introduction

In the geological context around the oil wells, the electric conductivity is a parameter that plays an important role. The Marine Controlled-Source Electromagnetic Method (CSEM) has emerged as a useful exploration technique for mapping offshore hydrocarbon reservoirs and characterizing gas hydrates bearing shallow sediments [4], [8], [9], [11], [13]. Large-scale 3D modeling of geophysical electromagnetic (EM) problems can easily overwhelm single core and modest multicore computing resources [22]. Therefore, the use of parallel computing resources to solve these problems is needed.

On the other hand, in order to obtain an accurate and efficient model of the EM field in complex geological structures the use of Edge Finite Element Method (EFEM) is needed. EFEM has the capability to model the frequency/time domain EM fields in the inhomogeneous complex bodies at any resistivities contrasts and at any survey types. EFEM satisfy, in an inherent way, the continuity constraint across the interface of the adjacent elements in the mesh.

This paper is about marine CSEM, linear vectorial edge basis functions and its parallel implementation on unstructured tetrahedral meshes. It's is divided as follows: Section 2 shortly describes the theory associated to CSEM and its importance as exploration tool. Section 3 is about linear edge elements and their basis vectorial functions. Emphasis is placed on aspects of orientation of geometries entities on unstructured meshes. Section 4 is dedicated to the main embarrassing parallel tasks that arise when implementing EFEM for CSEM. Section 5 describes the convergence test results in isotropic mediums and the performance aspects in terms of OpenMP communication. The last section is dedicated to conclusions and future work.

978-1-4799-7639-3/15/$31.00

II. Marine Controlled-source electromagnetic method

Marine Controlled-source Electromagnetic Methods (CSEM) are a type of geophysical strategies to study the subsurface electrical conductivity distribution with an ample range of applications. CSEM techniques can be divided into two groups depending on the domain in which collected data is interpreted: time domains (TDEM) or frequency domains (FDEM). In the case of oil prospecting, marine CSEM surveys are done predominantly using FDEM [12], [16]. In marine CSEM, also referred as seabed logging [11], a deep-towed electric dipole transmitter is used to produce a low frequency EM signal (primary field) which interacts with the electrically conductive Earth and induces eddy currents that become sources of a new EM signal (secondary field). The two fields, the primary and the secondary one, add up to a resultant field, which is measured by remote receivers placed on the seabed. Since the secondary field at low frequencies, for which displacement currents are negligible, depends primarily on the electric conductivity distribution of the ground, it is possible to detect thin resistive layers beneath the seabed by studying the received signal [15]. Operating frequencies of transmitters in CSEM may range between 0.1 and 10 Hz, and the choice depends on the dimensions of a model. In most studies, typical frequencies vary from 0.25 to 1 Hz, which means that for source-receiver offsets of 1012 km, the penetration depth of the method can extend to several kilometres below the seabed [1], [4], [5], [15]. The disadvantage of marine CSEM is its relatively low resolution compared to seismic imaging. Therefore, marine CSEM is almost always used in conjunction with seismic surveying as the latter helps to constrain the resistivity model. Figure 1

depicts the marine CSEM. Marine CSEM is nowadays a well-known geophysical prospecting tool in the offshore environment and a commonplace in industry, examples of that can be found in [7], [9], [16], [21], [25].

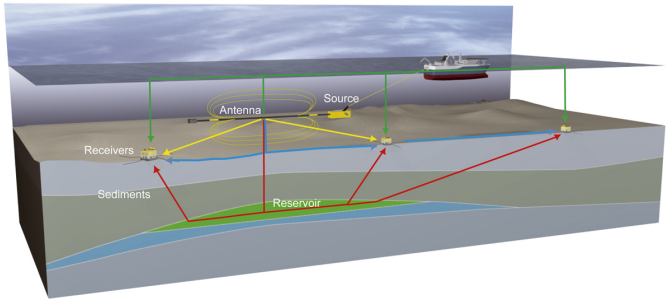

Fig. 1. Marine CSEM

Marine CSEM is a viable and cost-effective oil exploration technique. When integrated with other geophysics data, mainly seismic information, CSEM surveys are promising for adding value in shallow/deep waters. The outcomes and analysis of modeling with CSEM produce a more robust understanding of the prospection.

III. Linear edge elements

In the Finite Element modeling of EM fields both edge and nodal elements play an important role. Recently EFEM have gained an increase in popularity because its a cure for many difficulties that are encountered when attempting to solve EM field problems using Nodal Finite Elements [14], [18].

EFEM, or Nèdèlec Elements, have the main property that they ensure the continuity of tangential field components across an interface between different media, while leaving the normal field components free to jump across such interfaces [14], [10]. Because of this, Edge Elements can be used for modeling EM fields along interfaces between two different media. For the implementation of EFEM, the domain is discretised into subdomains using a mesh, which is commonly assembled from triangular in 2D, and hexahedral and tetrahedral in 3D. In our solution, we used unstructured tetrahedral meshes because they enable the representation of complex geological structures and allows local refinement in order to improve the solution's accuracy. Figure 2 shows the general form of linear Edge Elements on tetrahedral meshes, which has six unknowns or degrees of freedom (DOFs), one attached to each edge, and fourth vertices or nodes (red numbers).

Linear Edge Elements have following properties:

- DOFs are edge-associated, one per each grid edge.
- At interfaces, their tangential component is continuous, while the normal one is, in general, discontinuous.
- Are divergent-free.
- They do not yield conflicting conditions at points where the interface between two different media is not locally flat. The use of Edge Elements near sharp edges of subdomains in the configuration, or near re-entrant corners in the outer boundary of the domain of computation, "relaxes" the continuity requirements of the fields near those edges.
- As regards the economy (numerical efficiency), only six unknowns are required for each tetrahedron. The linear vectorial Lagrange elements, or any other consistently linear 3D-vector function over a tetrahedron, carries twelve unknowns, three at each of its four vertices.

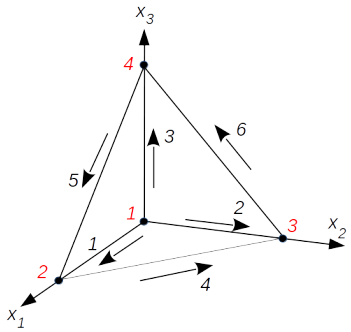

Fig. 2. An illustration of tetrahedron element. The red numbers indicates the node index and the black numbers is the index of edges.

Inside each element, a vector function is approximated by linear combination of shape functions associated with edges [14]. Therefore, within the element, the unknown function can be approximated as:

$$\phi^e(x,y,z) = a^e + b^e x + c^e y + d^e z \tag{1}$$

denoting the value of ϕ at the i-th node as ϕ_i^e, we have:

$$\begin{aligned}
\phi_1^e &= a^e + b^e x_1^e + c^e y_1^e + d^e z_1^e \\
\phi_2^e &= a^e + b^e x_2^e + c^e y_2^e + d^e z_2^e \\
\phi_3^e &= a^e + b^e x_3^e + c^e y_3^e + d^e z_3^e \\
\phi_4^e &= a^e + b^e x_4^e + c^e y_4^e + d^e z_4^e
\end{aligned}$$

volume of the element:

$$V^e = \frac{1}{6}\begin{vmatrix} 1 & 1 & 1 & 1 \\ x_1^e & x_2^e & x_3^e & x_4^e \\ y_1^e & y_2^e & y_3^e & y_4^e \\ z_1^e & z_2^e & z_3^e & z_4^e \end{vmatrix}$$

finding the coefficients a_i^e, b_i^e, c_i^e and d_i^e:

$$\begin{aligned}
a^e &= (6V^e)^{-1} \cdot (a_1^e\phi_1^e + a_2^e\phi_2^e + a_3^e\phi_3^e + a_4^e\phi_4^e) \\
b^e &= (6V^e)^{-1} \cdot (b_1^e\phi_1^e + b_2^e\phi_2^e + b_3^e\phi_3^e + b_4^e\phi_4^e) \\
c^e &= (6V^e)^{-1} \cdot (c_1^e\phi_1^e + c_2^e\phi_2^e + c_3^e\phi_3^e + c_4^e\phi_4^e) \\
d^e &= (6V^e)^{-1} \cdot (d_1^e\phi_1^e + d_2^e\phi_2^e + d_3^e\phi_3^e + d_4^e\phi_4^e)
\end{aligned}$$

Substituting the expressions for a^e, b^e, c^e and d^e back into equation 1 we obtain:

$$\phi^e(x,y,z) = \sum_{i=1}^{4} \Psi_i^e(x,y,z)\phi_i^e \tag{2}$$

TABLE I
EDGE DEFINITION FOR A TETRAHEDRAL ELEMENT

Edge i	Node i_1	Node i_2
1	1	2
2	1	3
3	1	4
4	2	3
5	4	2
6	3	4

where the interpolation functions $\Psi_i^e(x, y, z)$ are given by:

$$\Psi_i^e(x, y, z) = (6V^e)^{-1} \cdot (a_i^e + b_i^e x + c_i^e y + d_i^e z) \quad (3)$$

Equations 3 are the linear interpolation functions for the node tetrahedral elements, which can be denoted here as $(\rho_1^e, \rho_2^e, \rho_3^e, \rho_4^e)$. Therefore, the vectorial function for edge elements is defined as:

$$\Phi_{12} = \rho_1^e \nabla \rho_2^e - \rho_2^e \nabla \rho_1^e \quad (4)$$

since ρ_1^e is a linear function that varies from 1 at node 1 to zero at node 2 and ρ_2^e is a linear function that varies from 1 at node 2 to zero at node 1, Φ_{12} has a constant tangential component along edge $(1, 2)$. Further, since ρ_1^e vanishes along edges $(2, 3)$, $(2, 4)$, and $(3, 4)$ and ρ_2^e vanishes along edges $(1, 3)$, $(1, 4)$, and $(3, 4)$, Φ_{12} has no tangential component along these five edges. Furthermore, since ρ_1^e vanishes on the element facet defined by $(2, 3, 4)$ and ρ_2^e vanishes on the element facet defined by $(1, 3, 4)$, Φ_{12} has no tangential component on either of these facet as well. Its tangential components appears only on the element facets that contain edge $(1, 2)$, that is, the element facets $(1, 2, 3)$ and $(1, 2, 4)$. Thus, Φ_{12} possesses all the necessary properties to be a vector basis function for the edge field associated with edge $(1, 2)$. If we define this edge as edge 1, and ℓ_1^e as length of edge 1, we have:

$$\Psi_1^e = \Phi_{12}\ell_1^e = (\rho_1^e \nabla \rho_2^e - \rho_2^e \nabla \rho_1^e)\ell_1^e \quad (5)$$

Similarly, we obtain the vector basis function for edge *i* as:

$$\Psi_i^e = \Phi_{i1i2}\ell_i^e = (\rho_{i1}^e \nabla \rho_{i2}^e - \rho_{i2}^e \nabla \rho_{i1}^e)\ell_i^e \quad (6)$$

where the edge numbers and the associated nodes $i1$ and $i2$ are defined in table I.

Therefore, within a tetrahedral element *e*-th, the EM field can be represented as:

$$E_e = \sum_{n=1}^{6} E_n^e \Psi_n^e \quad (7)$$

where the EM field degree of freedom E_n^e is defined by a line integral along the edge n and Ψ_n^e is the edge basis function defined previously.

In order to obtain correct results and since the degrees of freedom are integrals over edges, is necessary get an uniform global orientation. Namely, a positive orientation for each edge in the mesh M is needed. To do that, our approach works as follows. If an edge adjoins two nodes n_i and n_j, the direction of the edge as going from node n_i to node n_j if $i < j$. This simple algorithm gives a unique orientation of each edge in the mesh M.

Figure 3 describes an isotropic 3D layer model and its meshing.

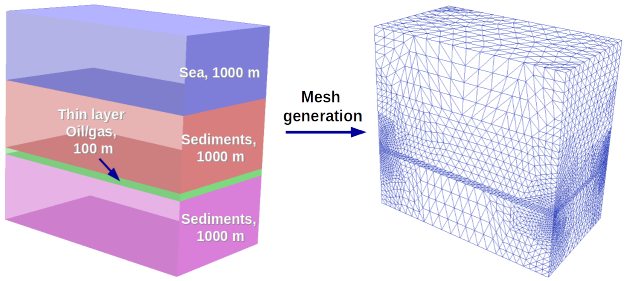

Fig. 3. 3D model and its meshing

In our experiments, the EM field is produced by a z-oriented dipole according with the formulation by [24]. This source transmits a carefully designed low-frequency EM signal into the subsurface. The main physical parameters for our test are described in table II.

TABLE II
MAIN PHYSICAL PARAMETERS

Parameter	Value
Domain dimensions (x,y,z)	3.5km, 2.5km, 3.100 km
Sea's electric resistivity	0.3 σ/m
Sediments electric resistivity	1 σ/m
Oil/gas electric resistivity	100 σ/m
Background electric resistivity	0.3 σ/m
Dipole position (x,y,z)	2.5km,1.2km,1.0km
Dipole current	1 C/m
Dipole frequency	.1 ω

IV. PARALLEL APPROACH FOR EDGE ELEMENTS

In order to meet the high computational cost of EFEM for EM fields, our solution is based on a shared memory parallel model defined by the OpenMP standard [23]. OpenMP has been widely adopted in the scientific computing community, and most vendors supports its Application Programming Interface (API) in their compiler suites. OpenMP offers not only parallel programs portability but, being based on directives, also a simple way to maintain a single code for the serial and parallel version of an application.

To exploit the advantages of geometric flexibility, our parallel approach is focused on embarrassingly parallel tasks, or tasks where does not exists dependency (or communication) between those parallel tasks. Namely, the minimum level of computing work is related with the edges in the mesh M. Therefore, our main parallel tasks are the following:

- T1: Mid-point computation for $edge_{i=1...n}$

- T2: Primary electric field computation for $edge_{i=1...n}$
- T3: Electric field projection over $edge_{i=1...n}$
- T4: Edge's length computation for $edge_{i=1...n}$
- T5: Direction vector for $edge_{i=1...n}$
- T6: Edge's orientation for $edge_{i=1...n}$

where i is the i-th edge in the mesh and n is the total number of edges in the mesh M. An outline of how the primary groups of functions in our implementation is given in Figure 4. All modules are based on traditional FEM codes. A more detailed explanation can be found in [6].

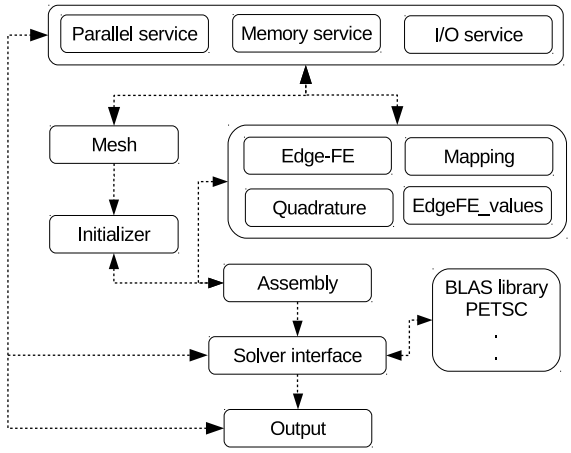

Fig. 4. Upper view of software stack

V. Results

To verify the accuracy and performance of our modeling, we used the model defined in figure 3. The experiments were performed on the Marenostrum supercomputer with two-8 cores Intel Xeon processors E52670 at 2.6 GHz per node. To increase the solution's accuracy, our implementation used an uniform refinement. In 3D domains, this approach results in 8 times more tetrahedral elements. Thus, in each refinement step the optimal increase in time would be 8.

Figure 5 shows the main property of our vectorial basis functions. For example it is easy to see that for the edge 1 (node 1 to node 2), the tangential component along this is constant while the normal component is discontinuous. This property is valid for the remaining edges.

In geophysical simulations with CSEM, the primary field is calculated analytically for a background layered-earth model. The secondary field is discretized using Edge Elements. Therefore, figure 6 depicts the ability of Edge Elements to interpolating the EM field produced by our dipole (source). Absolute and relative error per component are included. Both errors of the y-component are exactly zero since our dipole is z-directed.

Table III summarizes the results of our tests. The serial time and parallel time (both expressed in seconds) for each embarrassingly parallel tasks are included in function of the number of OpenMP threads. Here, parallel versions are significantly more efficient than serial versions.

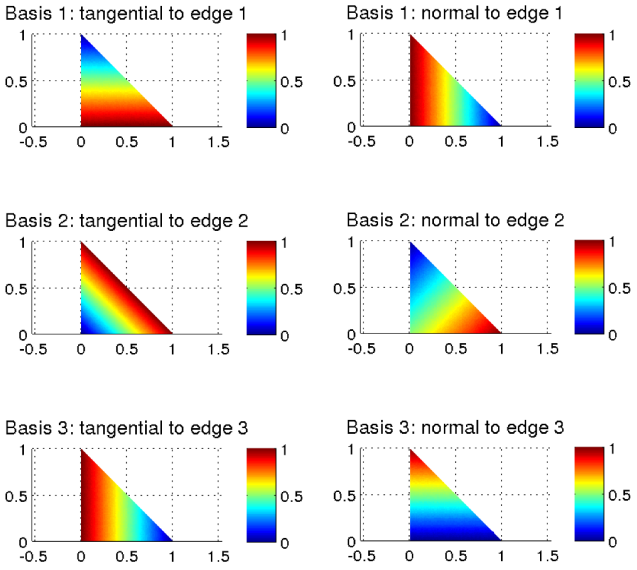

Fig. 5. Tangential and normal component of vectorial basis functions for each edge in one face of a tetrahedron.

In order to validate data from table III, we calculate the speed-up for the test 5. The results are show in table IV and figure 7. Our speed-up test considers only the computation time of embarrassingly parallel tasks. Figure 7 shows that we obtained a quasi linear speed-up. An important feature is that in our experiments the minimum execution time is not limited by the communication overhead. The latter issue is critical because if the computation time in each processor is smaller than the communication time, then the speed-up can saturate.

The convergence results are show in figure 8. We achieved a second order convergence, which is common in linear edge elements formulations without preconditioning.

VI. Conclusions

Marine CSEM, linear vectorial basis functions and its implementation on unstructured meshes were discussed. Marine CSEM is nowadays a well-known geophysical prospecting tool in the off-shore environment and a commonplace in industry. Then, we developed an Edge-based Finite Element algorithm to solve diffusive EM fields in 3D isotropic domains. The use of vectorial basis functions (edge basis) instead of the node basis function (Lagrange basis) results in the FEM break-through as a tool to model the EM response accurately. The edge basis automatically enforce the divergence free conditions for EM fields. Moreover, the continuity of the tangential EM is satisfied automatically as well. The use of unstructured meshes enables the representation of complex geological geometries, which brings us closer to modeling the EM response of realistic geological structures.

The developed code was tested for different meshes (based on uniform refinement) of a typical layered-earth model of the hydrocarbons reservoir. The performance and convergence results show that our parallel solution is profitable because the execution time is reduced without lose of accuracy. We

TABLE III
SUMMARY OF RESULTS

Task	Threads				
	Serial	2	4	8	16
Test 1: 384 elements, 604 edges					
T1	$9,000^{-03}$	5.100^{-03}	3.223^{-03}	1.648^{-03}	6.749^{-04}
T2	1.612^{-02}	8.221^{-03}	4.770^{-03}	3.114^{-03}	1.678^{-04}
T3	1.267^{-02}	3.125^{-03}	3.214^{-03}	1.914^{-03}	8.447^{-04}
T4	8.487^{-03}	4.710^{-03}	2.444^{-03}	1.621^{-03}	5.120^{-04}
T5	8.120^{-03}	4.220^{-03}	2.247^{-03}	1.126^{-03}	5.601^{-04}
T6	6.510^{-03}	3.712^{-03}	1.901^{-03}	8.236^{-04}	4.812^{-04}
Test 2: 3,072 elements, 4,184 edges					
Task	Threads				
	Serial	2	4	8	16
T1	7.230^{-02}	3.420^{-02}	1.620^{-02}	8.210^{-03}	4.101^{-03}
T2	1.293^{-01}	6.462^{-02}	2.881^{-02}	1.480^{-02}	7.880^{-02}
T3	1.017^{-01}	4.780^{-02}	2.170^{-02}	1.110^{-02}	6.101^{-03}
T4	6.820^{-02}	3.210^{-02}	1.100^{-02}	7.980^{-03}	3.879^{-03}
T5	6.530^{-02}	3.160^{-02}	1.241^{-02}	7.601^{-03}	3.980^{-03}
T6	5.241^{-02}	2.420^{-02}	1.270^{-02}	6.120^{-03}	3.022^{-03}
Test 3: 24,576 elements, 31,024 edges					
Task	Threads				
	Serial	2	4	8	16
T1	5.160^{-01}	2.980^{-01}	1.240^{-01}	7.280^{-02}	3.259^{-02}
T2	1.071^{+00}	5.140^{-01}	2.145^{-01}	1.177^{-01}	6.387^{-02}
T3	8.514^{-01}	4.010^{-01}	2.069^{-01}	1.001^{-01}	5.163^{-02}
T4	5.832^{-01}	2.417^{-01}	1.340^{-01}	6.981^{-02}	3.439^{-02}
T5	5.597^{-01}	2.290^{-01}	1.100^{-01}	6.890^{-02}	3.174^{-02}
T6	4.566^{-01}	2.011^{-01}	1.020^{-01}	5.204^{-02}	2.347^{-02}
Test 4: 196,608 elements, 238,688 edges					
Task	Threads				
	Serial	2	4	8	16
T1	4.651^{+00}	2.525^{+00}	1.062^{+00}	5.914^{-01}	3.040^{-01}
T2	8.298^{+00}	4.349^{+00}	2.107^{+00}	1.137^{+00}	5.486^{-01}
T3	6.534^{+00}	3.567^{+00}	1.833^{+00}	8.368^{-01}	4.284^{-01}
T4	4.388^{+00}	2.394^{+00}	1.297^{+00}	5.886^{-01}	2.943^{-01}
T5	4.200^{+00}	2.340^{+00}	1.350^{+00}	5.351^{-01}	2.825^{-01}
T6	3.376^{+00}	1.988^{+00}	8.661^{-01}	4.510^{-01}	2.310^{-01}
Test 5: 1,572,864 elements, 1,872,064 edges					
Task	Threads				
	Serial	2	4	8	16
T1	73.82^{+00}	37.27^{+00}	18.53^{+00}	9.781^{+00}	4.913^{+00}
T2	132.1^{+00}	67.08^{+00}	33.32^{+00}	17.52^{+00}	8.560^{+00}
T3	103.9^{+00}	53.97^{+00}	25.98^{+00}	13.44^{+00}	6.860^{+00}
T4	69.61^{+00}	36.93^{+00}	17.47^{+00}	9.013^{+00}	4.851^{+00}
T5	66.61^{+00}	35.66^{+00}	16.33^{+00}	8.894^{+00}	4.736^{+00}
T6	53.42^{+00}	27.71^{+00}	13.60^{+00}	7.286^{+00}	3.954^{+00}

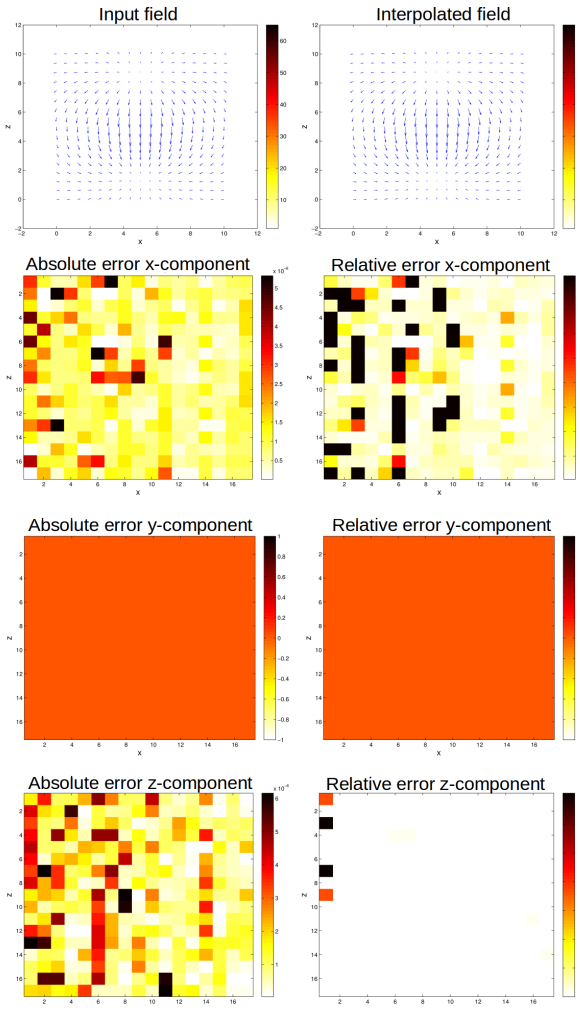

Fig. 6. Edge-element interpolation of an EM field produced by an z-oriented dipole. The absolute and relative error per component are included.

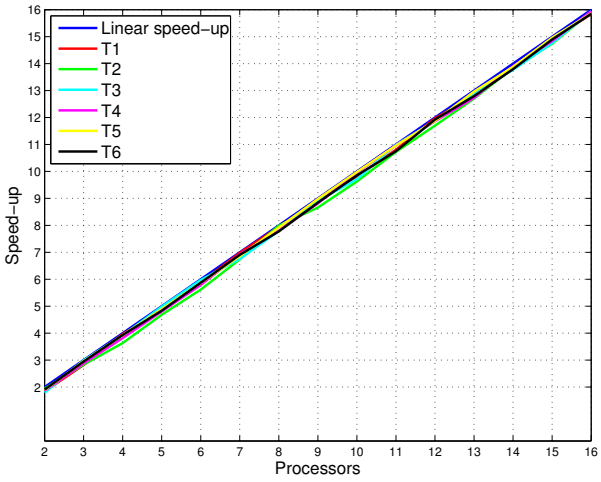

Fig. 7. Speed-up based in computation time for tasks in test 6 (1,572,864 elements with 1,872,064 edges).

achieved a quasi linear speed-up. This test considers only the computation time of embarrassingly parallel tasks. An important issue, is that in our experiments the minimum

TABLE IV
SPEED UP DATA: TEST 5

Threads	Tasks					
	1	2	3	4	5	6
2	1.8543	1.9173	1.9260	1.8140	1.9315	1.8483
3	2.8846	2.7385	2.7647	2.9656	2.8929	2.8931
4	3.9948	3.9712	3.7351	3.8860	3.8673	3.8925
5	4.9107	4.8373	4.7259	4.9229	4.8919	4.8609
6	5.8707	5.7332	5.8325	5.7993	5.9972	5.8225
7	6.8958	6.6265	6.8203	6.9207	6.8988	6.7433
8	7.9255	7.6756	7.9553	7.7491	7.9342	7.8050
9	8.8126	8.8062	8.7301	8.7686	8.9343	8.8920
10	9.8341	9.6973	9.8649	9.8908	9.9824	9.7754
11	10.830	10.833	10.938	10.860	10.877	10.963
12	11.925	11.611	11.730	11.805	11.951	11.983
13	12.881	12.604	12.771	12.766	12.963	12.977
14	13.825	13.654	13.735	13.829	13.948	13.955
15	14.813	14.844	14.914	14.839	14.943	14.912
16	15.866	15.818	15.798	15.908	15.918	15.918

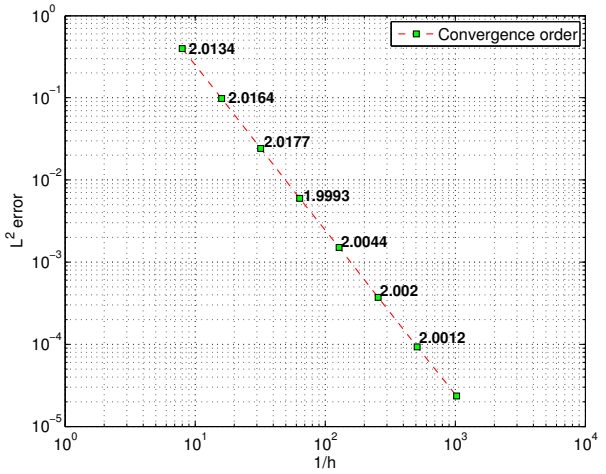

Fig. 8. Visualization of the convergence results of the linear Edge Elements in 3D. The ρ^2 error is plotted versus the mesh spacing h in y-axis.

execution time is not limited by the communication overhead.

Future work will be aimed in two lines. Firstly, at the implementation of an hybrid parallel model (MPI-OpenMP) to improve the computation time of the whole solution. Secondly, on adding more physical parameters such as topography, bathymetry and anisotropy.

ACKNOWLEDGMENT

This project has received funding from the European Union's Horizon 2020 research and innovation programme under the Marie Sklodowska-Curie grant agreement No. 644602.

Authors gratefully acknowledge the support from the Mexican National Council for Science and Technology (CONACYT).

REFERENCES

[1] Abubakar, A., Habashy, T., Druskin, V., Alumbaugh, D., Zerelli, A., Knizhnerman, L. (2006). Two-and-half-dimensional forward and inverse modeling for marine CSEM problems. In 2006 SEG Annual Meeting. Society of Exploration Geophysicists.

[2] Alumbaugh DL, Newman GA, Prevost L, Shadid JN (1996) Three dimensional, wideband electromagnetic modeling on massively parallel computers. Radio Sci 31:123.

[3] Alumbaugh DL, Newman GA (1997) 3-D massively parallel electromagnetic inversionpart II. Anual Crosswell Exp Geophys J Int 128:355363.

[4] Boulaenko, M., Hesthammer, J., Vereshagin, A., Gelting, P., Davies, R., and Wedberg, T. (2007). Marine csem technologythe luva case. Houston Geological Society.

[5] Carazzone, J. J., Burtz, O. M., Green, K. E., Pavlov, D. A., Xia, C. (2005). Three dimensional imaging of marine CSEM data. In 2005 SEG Annual Meeting. Society of Exploration Geophysicists.

[6] Castillo, O., dela Puente, J., Puzyrev, V., Cela, J. M. (2015). Assessment of edge-based finite element technique for geophysical electromagnetic problems: efficiency, accuracy and reliability. Proceedings of the 1st Pan-American Congress on Computational Mechanics and XI Argentine Congress on Computational Mechanics. CIMNE, pp. 984-995.

[7] Commer, M., Newman, G. A. (2008). New advances in threedimensional controlledsource electromagnetic inversion.

[8] Constable, S. (2006). Marine electromagnetic methodsa new tool for offshore exploration. The Leading Edge, 25(4):438444.

[9] Constable, S. (2010). Ten years of marine csem for hydrocarbon exploration. Geophysics, 75(5):75A6775A81.

[10] Chung, Y., Son, J. S., Lee, T. J., Kim, H. J., Shin, C. (2014). Three-dimensional modelling of controlledsource electromagnetic surveys using an edge finiteelement method with a direct solver. Geophysical Prospecting, 62(6), 1468-1483.

[11] Eidesmo, T., Ellingsrud, S., MacGregor, L., Constable, S., Sinha, M., Johansen, S., Kong, F. & Westerdahl, H., 2002. Sea bed logging (SBL), a new method for remote and direct identification of hydrocarbon filled layers in deepwater areas, First Break, 20, 144152.

[12] Grayver, A. V. (2013). Three-dimensional controlled-source electromagnetic inversion using modern computational concepts. PhD thesis, Freie Universitt Berlin.

[13] Hanif, N. H. H. M., Hussain, N., Yahya, N., Daud, H., Yahya, N., and Noh, M.(2011). 1d modeling of controlled-source electromagnetic (csem) data using finite element method for hydrocarbon detection in shallow water. In Proceedings of the International MultiConference of Engineers and Computer Scientists.

[14] Jin, J. (2002). The Finite Element Method in Electromagnetics. Wiley, New York, Second edition.

[15] Koldan, J. (2013). Numerical solution of 3-D electromagnetic problems in exploration geophysics and its implementation on massively parallel computers. PhD thesis, Polytechnic University of Catalonia.

[16] Key, K. (2012). Marine electromagnetic studies of seafloor resources and tectonics. Surveys in geophysics, 33(1):135167.

[17] McCann, D.M., Eddleston, M., Fenning, P.J., Reeves, G.M. (1997). Modern Geophysics in Engineering Geology. Geological Society Engineering Geology Special Publication.

[18] Mur, G. (1994). Edge elements, their advantages and their disadvantages. Magnetics, IEEE Transactions on, 30(5), 3552-3557.

[19] Nèdèlec, J. C. 1980). Mixed finite elements in ℜ3. Numerische Mathematik, 35(3), 315-341.

[20] Newman GA, Alumbaugh DL (1997) 3-D massively parallel electromagnetic inversionpart I theory. Geophys J Int 128:345354

[21] Newman, G. A., Commer, M., Carazzone, J. J. (2010). Imaging CSEM data in the presence of electrical anisotropy. Geophysics, 75(2), F51-F61.

[22] Newman, G. A. (2014). A Review of high-performance computational strategies for modeling and imaging of electromagnetic induction data. Surveys in Geophysics, 35(1), 85-100.

[23] OpenMP Architecture Review Board (2015). OpenMP application program interface. Version 4.0.

[24] Vozoff, K. (1991). Electromagnetic methods in applied geophysics.

[25] Weiss, C. J., Newman, G. A. (2002). Electromagnetic induction in a fully 3-D anisotropic earth. Geophysics, 67(4), 1104-1114.